Variation tendencies of shape memory alloys surface relief as a function of training-cycling parameters

M.-G. SURU[a], C. MOROŞANU[b], L.-G. BUJOREANU[a,*]
[a] *Faculty of Materials Science and Engineering, The "Gheorghe Asachi" Technical University of Iaşi, Bd. D. Mangeron 67, 700050 Iaşi, Romania*
[b] *Department of Mathematics, Alexandru Ioan Cuza University, Bd. Carol I-11, 700506 Iasi, Romania*

Lamellar specimens of Cu-Zn-Al Shape Memory Alloy (SMA) were trained in bending under as much as 500 cycles, until two-way shape memory effect (2WE) was obtained. Trained specimens were further tested by means of a hydraulic installation where, heating-cooling cycles were performed in oil conditions. Considering that the lower concave surface of the specimens was kept in compressed state while the upper convex surface was kept in elongated state, this study reveals the variation tendencies of the width and height of martensite plates as a function of training-cycling parameters, while considering the effects of different loading modes, namely compression and elongation. The convex and concave regions, of the Cu-Zn-Al specimens in air-trained or oil-cycled conditions after being subjected to large number of cycles, were metallographically prepared and analysed by atomic force microscopy (AFM). The study comprised comparative investigations of 2D and 3D representative profiles corroborated with numerical analysis of large number of recorded data, in order to reveal the effects of the number of cycles, loading mode and environmental conditions, on the general variation tendency of the surface relief of martensite plates.

(Received February 5, 2014; accepted March 13, 2014)

Keywords: Shape memory alloys, Training-cycling, Surface relief, Martensite plates, Statistical evaluation

1. Introduction

Shape memory alloys (SMAs) belong to a class of shape memory materials (SMMs), which have the ability to ''memorise" a previous form, from their thermomechanical history, when subjected to certain stimulus [1]. ''Shape memory" is the term used to describe the main property of SMMs [2]. SMAs have been used in industrial fields [3] for their one-way shape memory effect (1WE) [4], pseudoelasticity (PE) [5] and two-way shape memory effect 2WE [6]. Any SMA with 1WE can revert to its original shape once the low temperature stress-induced martensite phase is heated to A_f (austenite transformation finish temperature). Any SMA with 2WE [7] has the potential to change its shape once the low temperature martensite phase is heated to the high-temperature austenite phase, and to revert to its original shape while being cooled back to martensite.

Many alloys exhibit shape memory effect, but Ni–Ti-based shape memory alloys, have to date, provided the best combination of materials properties for most commercial applications [8]. On the other hand, Cu–Zn–Al alloys provide a more economical alternative to Ni–Ti. Shape memory properties in copper-base alloys [9] are associated with the thermoelastic martensitic transformation taking place from hard austenite phase (β_2) to soft martensite (β'_2) [10]. The transformation occurs without diffusion [11], and, consequently, martensite inherits a part of long-range order of the β phase [12]. The β_2 CuZnAl phase, at high temperatures, displays a body centred cubic (bcc) disordered structure [13]. However, in the interest range of temperatures it exhibits a long-range ordered structure called B2 [14]. The martensitic product phase has a 9R structure [15], which can be well described as an face centred tetragonal (fct) lattice with stacking faults every three planes. Martensitic transformation can be induced by cooling [16], spontaneous transformation, or by applying mechanical stress [17]. During cooling, transformation starts at a critical temperature Ms and completes at M_f [18], below which, theoretically, the crystal is purely martensitic. On heating, the reverse martensitic transformation starts at A_s temperature and ends at A_f. When applying a mechanical stress, such as tension or compression, at temperature above A_f, stress induced martensitic transformation starts at a critical stress level, and ends at almost constant stress, when a critical deformation is reached [19]. However, this stress-induced martensite is unstable at temperatures above A_f, and therefore reverse phase transformation to austenite occurs, at a lower stress level, during unloading [20]. Thus, a hysteretic loop is formed, in cooling/heating cycles [21] as well as in isothermal loading/unloading cycles [22].

The aim of the present paper is to determine the general variation tendencies of SMA surface relief as a function of number of cycles, heating-cooling environment and loading mode (elongation and compression).

2. Materials and methods

Cu-15 Zn-6 Al (mass. %) SMA specimens of were hot rolled [23], heat treated [24] and trained in air during up to 500 cycles, until obtaining 2WE, as previously described [25]. 2WE air-trained actuators were tested in a hydraulic installation, where heating-cooling cycles were performed in oil environment, without exceeding A_f = 404 K [26]. From the most solicited areas of both air-trained and oil-cycled specimens, fragments were cut with particular care to differentiate between convex region which was mostly subjected to tension and concave region subjected mainly to compression. These fragments were further encapsulated, ground and electro-polished using an AX-D1 electrolytic polisher as described in a previous paper [27].

The specimens were analysed with an Atomic Force Microscope (AFM) type NanoSurf easyScan, equipped with silicon SPM cantilevers and easyScope video camera, at a scanning rate of 2×10^{-1} s per line, as previously detailed [28]. Aiming to perform numerical analysis [29], on the surface of each specimen under study five characteristic groups of primary plates with length larger than 50 µm, in different grains, were selected and five parallel plates within each group were measured [30].

On AFM micrographs, the widths and heights of martensite plates were measured with nanometre-precision on elongated (convex) and compressed (concave) surfaces of the specimens, by means of AFM software.

The obtained values of width and height, for each surface in part, were used for numerical analysis [31], performed by means of MATLAB software, using spline interpolation of surface relief geometrical measurement data [32].

3. Results and discussion

3.1 Structural analysis by AFM

The typical structure of martensite plates recorded on analysed specimens in initial state, after hot rolling and heat treatment but before training, is illustrated in Fig. 1. It can be noticed that martensite plates are rather coarse, the average values of measured width and height being 187 and 167 nm, respectively. Fig. 1 will be further used for and comparative reasons, namely the general aspect for qualitative comparisons and measured data for quantitative evaluations.

The qualitative effects of the number of air-training cycles (100 to 500) and loading mode (elongation or compression) can be observed by analysing Fig. 2. It is obvious that there are two variation tendencies, depending on the number of air-training cycles and loading mode:

- a refining tendency of both heights and widths of primary martensite plates, with increasing the number of air-training cycles;
- unlike elongation mode, which contributed to the diminution of martensite plate widths and heights, compression mode maintained these surface relief parameters to rather elevated values.

For this reason, the refining effect of the number of air-training cycles was more obvious for elongation than for compression.

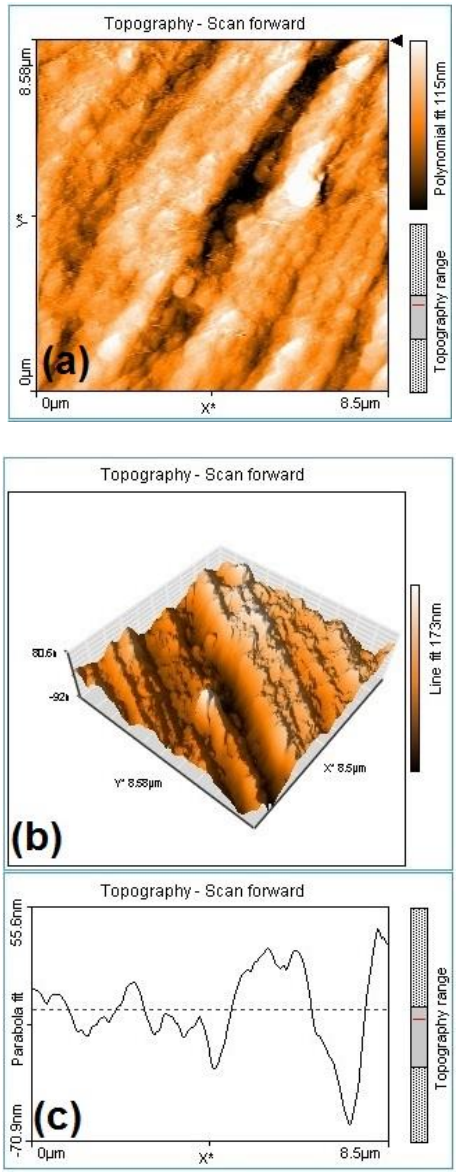

Fig. 1. AFM micrographs illustrating the typical initial structure of untrained specimens: (a) 2-D image; (b) 3-D image; (c) surface relief profile.

After oil-cycling, the effects observed in Fig. 2 were maintained, as illustrated in Fig. 3. However, in this case, the general structural aspect was altered, due to the formation of two different systems of martensite plates:

- a system of large primary plates, which are obviously larger and more numerous;
- isolated groups of secondary martensites plates, with smaller dimensions, which have different orientation as compared to primary plates.

As previously pointed out, the formation of secondary martensite plate systems could be ascribed to the so-called temperature memory effect, which was caused by heating interruption in previous cycle [23].

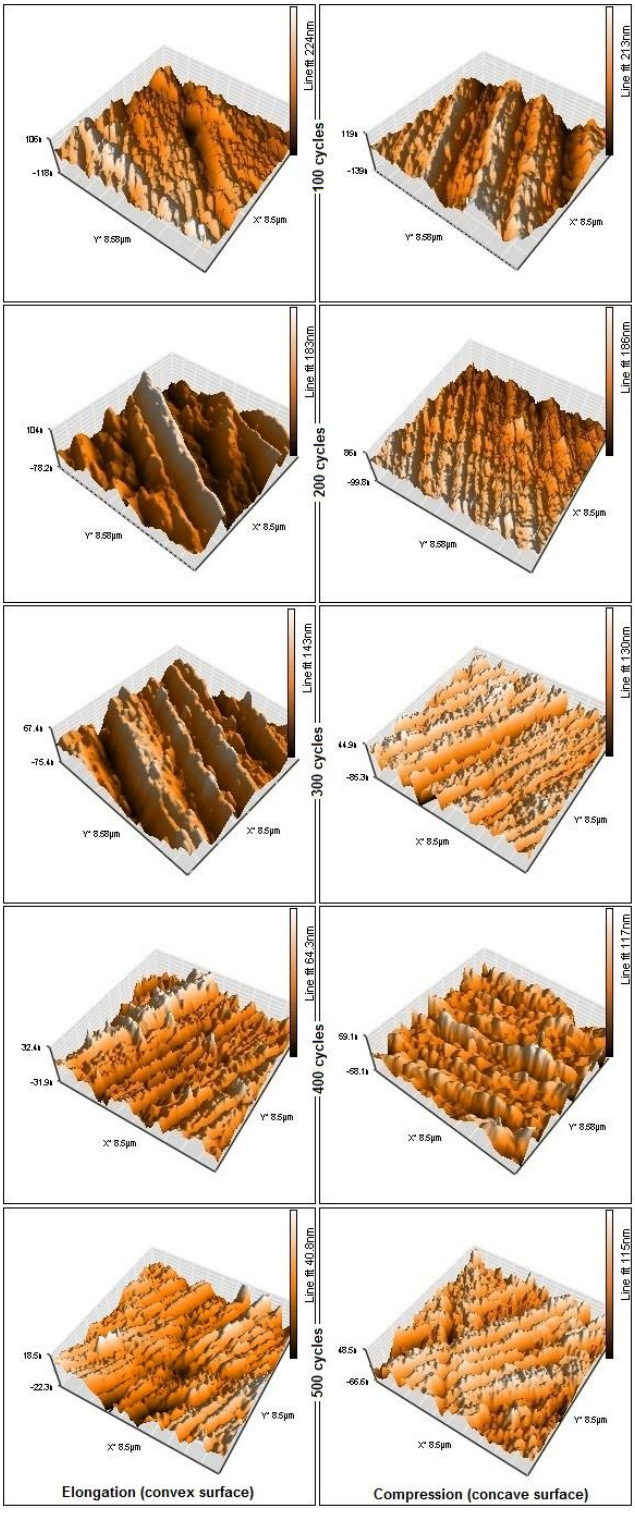

Fig. 2. 3-D AFM micrographs of air-trained specimens illustrating the effects of air-training cycles and loading mode (elongation-compression) on the surface relief of primary martensites plates.

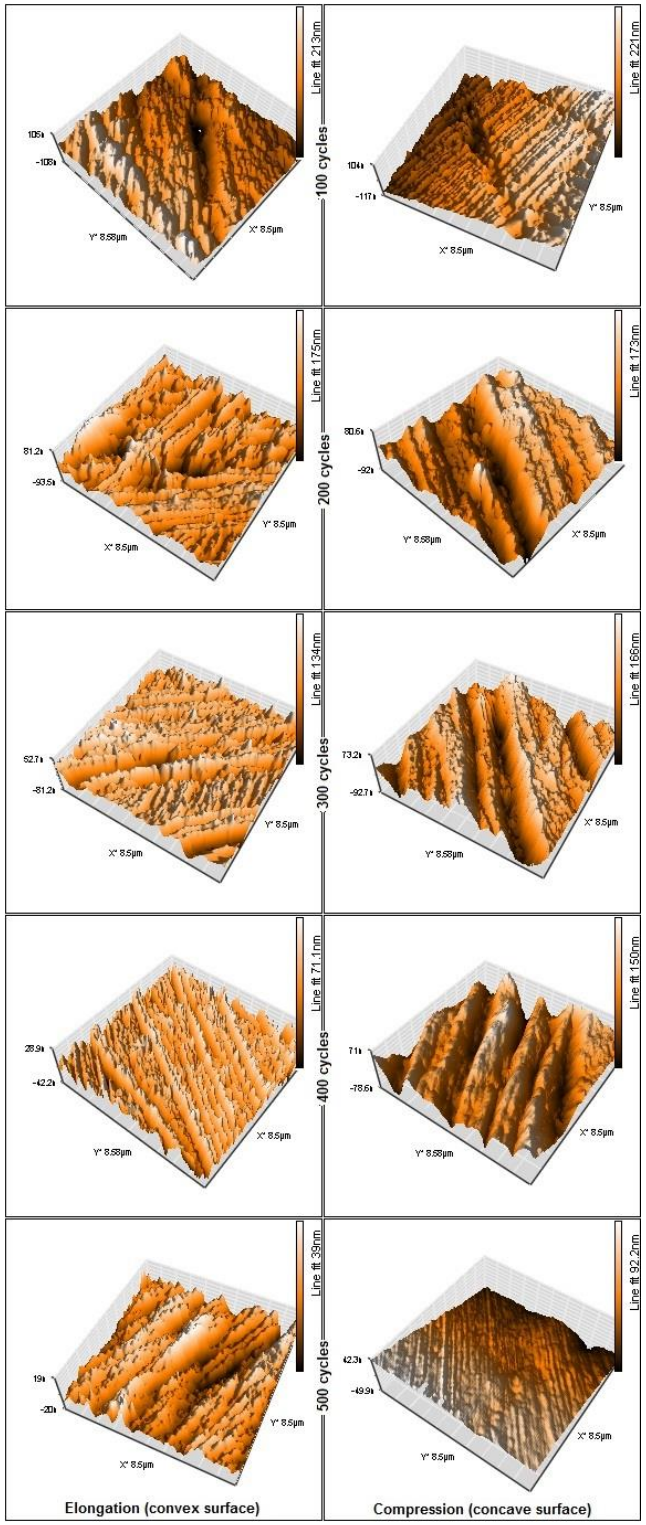

Fig. 3. 3-D AFM micrographs of oil-cycled specimens illustrating the alteration of the effects of air-training cycles and loading mode, on surface relief of primary martensites plates.

When comparing Figs. 2 and 3, the effects of training cycles and loading mode are more obvious. A fair evaluation of martensite plate heights is given by the dimensional bar on upper right–side of each micrograph.

Thus, general relief depth tend to decrease with increasing the number of cycles and to become larger from compression as compared to elongation mode, as illustrated by the typical relief variations shown in Fig. 4.

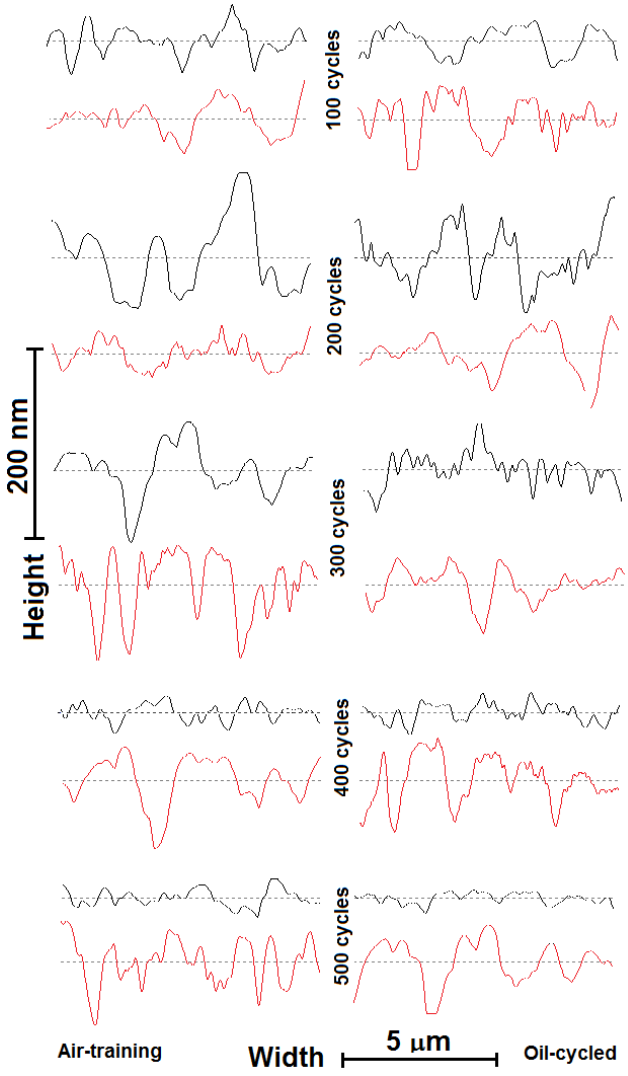

Fig. 4. Typical surface relief profiles recorded by AFM, illustrating the cumulated effects of the number of air-training cycles and oil-cycling. The upper black profiles correspond to the surfaces subjected to elongation (convex) and lower red profiles to compression (concave)

Table 1. Descriptive data of air-trained specimens.

Area	N	Mean	Std. Devi-ation	Std. Error	95% Confidence Interval for Mean		Min	Max	p
					Lower Bound	Upper Bound			
width CuZnAl x 0 cycles (nm)									
elong.	125	187.50	56.48	5.05	177.50	197.50	95.00	330.0	1,000
compr.	125	187.51	56.48	5.05	177.51	197.51	95.00	330.0	
Total	250	187.50	56.37	3.56	180.48	194.53	95.00	330.0	
height CuZnAl x 0 cycles (nm)									
elong.	125	167.97	49.11	4.39	159.28	176.67	90.00	255.0	1,000
compr.	125	167.97	49.11	4.39	159.28	176.67	90.00	255.0	
Total	250	167.97	49.02	3.10	161.87	174.08	90.00	255.0	
width CuZnAl x 100 cycles (nm)									
elong.	125	184.33	51.81	4.63	175.16	193.50	67.00	298.7	0,775
compr.	125	186.55	69.56	6.22	174.23	198.86	87.00	315.0	
Total	250	185.44	61.22	3.87	177.81	193.06	67.00	315.0	
height CuZnAl x 100 cycles (nm)									
elong.	125	94.85	32.32	2.89	89.13	100.57	63.19	234.5	**0,001**
compr.	125	149.07	62.59	5.60	137.99	160.15	83.00	244.0	
Total	250	121.96	56.65	3.58	114.90	129.02	63.19	244.0	
width CuZnAl x 200 cycles (nm)									
elong.	125	181.30	39.69	3.55	174.27	188.32	62.00	245.0	0,753
compr.	125	183.65	73.57	6.58	170.63	196.68	80.00	290.0	
Total	250	182.47	59.00	3.73	175.12	189.82	62.00	290.0	
height CuZnAl x 200 cycles (nm)									
elong.	125	90.10	46.94	4.20	81.79	98.41	43.19	205.0	**0,001**
compr.	125	144.26	60.52	5.41	133.54	154.97	78.00	235.0	
Total	250	117.18	60.47	3.82	109.65	124.71	43.19	235.0	
width CuZnAl x 300 cycles (nm)									
elong.	125	130.65	27.99	2.50	125.70	135.61	60.00	199.1	**0,001**
compr.	125	179.41	63.68	5.70	168.14	190.69	76.00	252.0	
Total	250	155.03	54.83	3.47	148.20	161.86	60.00	252.0	
height CuZnAl x 300 cycles (nm)									
elong.	125	78.24	27.57	2.47	73.36	83.12	33.19	165.9	**0,001**
compr.	125	137.12	53.84	4.82	127.58	146.65	70.56	211.0	
Total	250	107.68	51.89	3.28	101.21	114.14	33.19	211.0	
width CuZnAl x 400 cycles (nm)									
elong.	125	91.96	32.50	2.91	86.20	97.71	45.00	150.0	**0,001**
compr.	125	155.66	44.68	4.00	147.75	163.57	70.00	221.9	
Total	250	123.81	50.39	3.19	117.53	130.09	45.00	221.9	
height CuZnAl x 400 cycles (nm)									
elong.	125	68.12	36.42	3.26	61.67	74.56	33.10	131.0	**0,001**
compr.	125	120.89	50.80	4.54	111.90	129.88	63.00	200.6	
Total	250	94.50	51.42	3.25	88.10	100.91	33.10	200.6	
width CuZnAl x 500 cycles (nm)									
elong.	125	70.68	29.75	2.66	65.41	75.95	33.19	132.7	**0,001**
compr.	125	122.73	42.68	3.82	115.17	130.29	60.00	200.9	
Total	250	96.70	45.03	2.85	91.10	102.31	33.19	200.9	
height CuZnAl x 500 cycles (nm)									
elong.	125	53.13	19.24	1.72	49.72	56.53	33.10	100.5	**0,001**
compr.	125	106.41	45.65	4.08	98.33	114.50	57.00	185.0	
Total	250	79.77	43.99	2.78	74.29	85.25	33.10	185.0	

From the evolutions of surface profiles it appears that martensite plates from compressed areas are less responsive to the variation of the number of training cycles, as compared to elongated areas.

In order to evaluate the quantitative effects of the number of air-training cycles, loading mode, (elongation or compression) and oil cycling, numerical analysis was performed, as specified in the following.

3.2 Numerical analysis of AFM data

Table 1 lists the results of numerical analysis of the 3000 data (N) corresponding to air-training. It contains maximum, minimum and mean values of width and height as well as standard deviations and errors, together with lower and upper limits of 95 % confidence interval for the mean values, for elongation and compression.

In initial state no obvious differences exist between surface relief values measured in elongated and compressed areas. Width variation range was between 95-330 nm while height range was 90-225 nm. After 100 air-training cycles, width variation range became 67-315 nm with larger values in compressed areas, while height variation range was 63.1-244 nm. In the same trend, these intervals become lower and lower, down to 33,1-200.9 nm, in the case of width and to 33,1-185 nm, in the case of heights, after 500 air-training cycles.

Oil-cycling cause the occurrence of secondary martensite populations while the dimensions of primary martensite plates were influenced, as well. The results of numerical analysis of the 3000 representative data, measured after oil-cycling are listed in Table 2, where the same notations were used. A simple comparison of mean values allows noticing that oil-cycling also contributed to moderate diminution of martensite surface relief.

Table 2. Descriptive data of oil-cycled specimens.

Area	N	Mean	Std. Devi-ation	Std. Error	95% Confidence Interval for Mean		Min	Max	p
					Lower Bound	Upper Bound			
width CuZnAl x 0 cycles (nm)									
elong.	125	187.50	56.48	5.05	177.50	197.50	95.00	330.0	1,000
compr.	125	187.50	56.48	5.05	177.50	197.50	95.00	330.0	
Total	250	187.50	56.37	3.57	180.48	194.52	95.00	330.0	
height CuZnAl x 0 cycles (nm)									
elong.	125	167.97	49.11	4.39	159.28	176.67	90.00	255.0	1,000
compr.	125	167.97	49.11	4.39	159.28	176.67	90.00	255.0	
Total	250	167.97	49.02	3.10	161.87	174.08	90.00	255.0	
width CuZnAl x 100 cycles (nm)									
elong.	125	155.07	59.80	5.35	144.48	165.65	79.00	298.7	0,901
compr.	125	154.12	61.43	5.49	143.24	164.99	89.00	309.0	
Total	250	154.59	60.50	3.83	147.06	162.13	79.00	309.0	
height CuZnAl x 100 cycles (nm)									
elong.	125	119.96	43.44	3.89	112.27	127.65	73.19	220.0	**0,001**
compr.	125	149.23	57.58	5.15	139.04	159.42	85.00	220.8	
Total	250	134.60	52.97	3.35	128.00	141.20	73.19	220.8	
width CuZnAl x 200 cycles (nm)									
elong.	125	123.85	48.92	4.38	115.19	132.51	68.00	250.0	**0,014**
compr.	125	138.87	47.19	4.22	130.51	147.22	79.00	270.0	
Total	250	131.36	48.55	3.07	125.31	137.41	68.00	270.0	
height CuZnAl x 200 cycles (nm)									
elong.	125	94.38	35.96	3.22	88.01	100.74	55.00	208.0	**0,001**
compr.	125	135.06	47.42	4.24	126.66	143.45	71.00	195.9	
Total	250	114.72	46.68	2.95	108.90	120.53	55.00	208.0	
width CuZnAl x 300 cycles (nm)									
elong.	125	100.14	35.49	3.17	93.86	106.42	57.01	199.1	**0,001**
compr.	125	123.03	46.61	4.17	114.77	131.28	68.00	230.0	
Total	250	111.58	42.90	2.71	106.24	116.93	57.01	230.0	
height CuZnAl x 300 cycles (nm)									
elong.	125	79.60	27.24	2.44	74.78	84.42	45.00	165.9	**0,001**
compr.	125	119.41	46.72	4.18	111.14	127.68	65.00	180.0	
Total	250	99.51	43.06	2.72	94.14	104.87	45.00	180.0	
width CuZnAl x 400 cycles (nm)									
elong.	125	86.10	39.73	3.55	79.06	93.13	49.00	170.0	**0,001**
compr.	125	109.06	44.41	3.97	101.20	116.92	52.00	200.0	
Total	250	97.58	43.59	2.76	92.15	103.01	49.00	200.0	
height CuZnAl x 400 cycles (nm)									
elong.	125	67.13	27.02	2.42	62.34	71.91	40.00	140.0	**0,001**
compr.	125	101.25	31.32	2.80	95.70	106.79	49.00	160.0	
Total	250	84.19	33.83	2.14	79.97	88.40	40.00	160.0	
width CuZnAl x 500 cycles (nm)									
elong.	125	64.37	32.10	2.87	58.68	70.05	33.19	132.7	**0,001**
compr.	125	101.31	32.69	2.92	95.52	107.10	43.19	132.7	
Total	250	82.84	37.26	2.36	78.20	87.48	33.19	132.7	
height CuZnAl x 500 cycles (nm)									
elong.	125	50.55	20.30	1.82	46.96	54.15	33.10	100.5	**0,001**
compr.	125	85.59	32.70	2.92	79.80	91.38	39.10	120.0	
Total	250	68.07	32.34	2.05	64.05	72.10	33.10	120.00	

Based on the data displayed in the two tables, the continuous variation tendencies of the two different surface relief characteristics – width and height – were plotted, by means of spline approximation, as shown in Figs. 5 and 6, respectively.

The symbols correspond to mean values of the data measured for initial state and the five different numbers of air-training cycles.

Referring to Fig.5, the refining tendency of martensite plate widths is obvious, with increasing the number of air-training cycles. Conversely, when comparing the data corresponding to air-training and to oil-cycling it is evident that the latter were lower, both for elongated and compressed areas. Spline approximation enables to derive a general variation tendency of martensite plate width, which integrates the data for both loading modes and cycling environment.

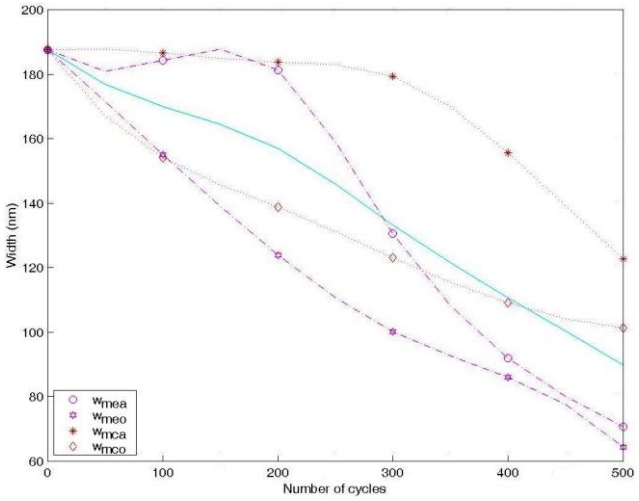

Fig. 5. Continuous variation tendencies of martensite plate widths for the mean values of elongated areas after air- training (w_{mea}) and oil-cycling (w_{meo}) and the same results for compression areas (w_{mca} and w_{mco}, respectively). Isolated values correspond to measured data and central solid line displays general variation tendency of martensite plate widths.

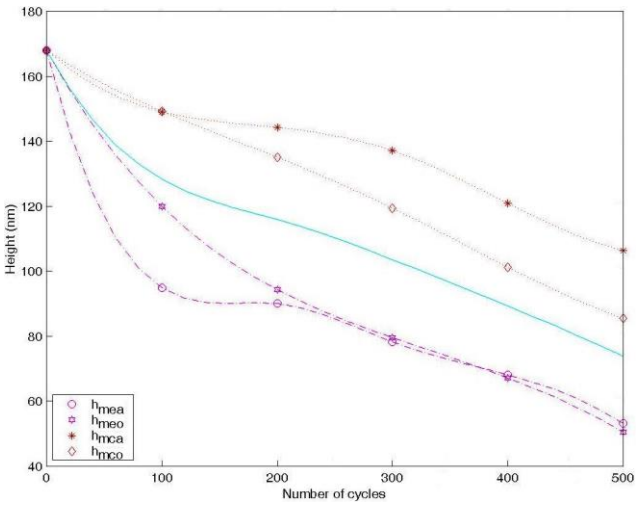

Fig. 6. Continuous variation tendencies of martensite plate heights for the mean values of elongated areas after air- training (h_{mea}) and oil-cycling (h_{meo}) and the same results for compression areas (h_{mca} and h_{mco}, respectively). Isolated values correspond to measured data and central solid line displays general variation tendency of martensite plate widths.

By means of spline interpolation, general relationships were determined for each of the above continuous variation tendencies of martensite plate widths and heights, after air-training, oil-cycling, in elongated or compressed areas [29]:

$$S_{(x)} = a_j + b_j(x - x_j) + c_j(x - x_j)^2 + d_j(x - x_j)^3 \qquad (1)$$

where $x_j \le x \le x_{j+1}; j = 0, 1, \dots, n-1$

The values of the above coefficients corresponding to the variation tendencies of martensite plate width and height, illustrated in Figs. 5 and 6, both for measured parameters (dash lines) and general tendency (solid) are listed in Tables 3 and 4, respectively.

Table 3. Spline coefficients for martensite plate width variation tendencies, illustrated in Fig. 5.

Environment	Load mode	No of cycles x_i	Spline coefficients			
			a_i	b_i	c_i	d_i
Air-training	Elongation	100	187.50	-0.07	0.00	0.36×10^{-5}
		200	184.33	0.04	1.08×10^{-2}	-1.79×10^{-5}
		300	181.30	-0.28	-4.27×10^{-3}	0.20×10^{-4}
		400	130.65	-0.53	1.75×10^{-3}	-0.29×10^{-5}
		500	91.96	-0.27	0.87×10^{-3}	0.28×10^{-5}
	Compression	100	187.51	-0.21×10^{-2}	0.00	-0.75×10^{-6}
		200	186.55	-2.47×10^{-2}	-0.22×10^{-3}	1.83×10^{-6}
		300	183.65	-1.51×10^{-2}	0.32×10^{-3}	-5.95×10^{-6}
		400	179.41	-0.13	-1.46×10^{-3}	3.80×10^{-6}
		500	155.66	-0.31	-0.32×10^{-3}	1.08×10^{-6}
Oil-cycling	Elongation	100	187.50	-0.33	0.00	0.1×10^{-7}
		200	155.07	-0.32	0.21×10^{-5}	1.17×10^{-6}
		300	123.85	-0.29	0.35×10^{-3}	1.59×10^{-6}
		400	100.14	-0.17	0.83×10^{-3}	-0.54×10^{-5}
		500	86.10	-0.16	-0.78×10^{-3}	0.26×10^{-5}
	Compression	100	187.50	-0.38	0.00	0.49×10^{-5}
		200	154.12	-0.24	0.15×10^{-2}	-0.64×10^{-5}
		300	138.87	-0.13	-0.45×10^{-3}	0.20×10^{-5}
		400	123.03	-0.16	0.15×10^{-3}	0.10×10^{-5}
		500	109.06	-0.11	0.43×10^{-3}	-0.14×10^{-5}
General variation tendency		100	187.5	-0.19	0	0.19×10^{-5}
		200	170.02	-0.13	0.58×10^{-3}	0.53×10^{-5}
		300	156.91	-0.17	-0.1×10^{-3}	0.44×10^{-5}
		400	133.31	-0.24	0.31×10^{-3}	-0.9×10^{-6}
		500	110.69	-0.21	0.47×10^{-4}	-0.16×10^{-6}

Table 4 Spline coefficients for martensite plate height variation tendencies, illustrated in Fig. 6.

Environment	Load mode	No of cycles x_i	Spline coefficients			
			a_i	b_i	c_i	d_i
Air-training	Elongation	100	167.97	-0.92	0.00	0.19×10^{-4}
		200	94.85	-0.35	0.57×10^{-2}	-0.26×10^{-4}
		300	90.10	-0.21×10^{-2}	-0.22×10^{-2}	0.10×10^{-4}
		400	78.24	-0.14	0.81×10^{-3}	-0.46×10^{-5}
		500	68.12	-0.11	-0.57×10^{-3}	0.19×10^{-5}
	Compression	100	167.97	-0.23	0.00	0.38×10^{-5}
		200	149.07	-0.11	0.11×10^{-2}	-0.47×10^{-5}
		300	144.26	-0.03	-0.29×10^{-3}	-0.13×10^{-5}
		400	137.12	-0.13	-0.69×10^{-3}	0.33×10^{-5}
		500	120.89	-0.16	0.30×10^{-3}	-0.10×10^{-5}
Oil-cycling	Elongation	100	167.97	-0.53	0.00	0.53
		200	119.96	-0.37	0.16×10^{-2}	-0.41×10^{-5}
		300	94.38	-0.18	0.37×10^{-3}	-0.07×10^{-5}
		400	79.60	-0.12	0.17×10^{-2}	-0.17×10^{-5}
		500	67.13	-0.14	-0.35×10^{-2}	0.12×10^{-5}
	Compression	100	167.97	-0.20	0.00	0.13×10^{-5}
		200	149.23	-0.16	0.38×10^{-3}	-0.18×10^{-5}
		300	135.06	-0.14	-0.15×10^{-3}	-0.19×10^{-6}
		400	119.41	-0.18	-0.21×10^{-3}	0.15×10^{-5}
		500	101.25	-0.17	0.24×10^{-3}	-0.80×10^{-6}
General variation tendency		100	167.97	-0.46	0	-0.73×10^{-5}
		200	128.27	-0.25	0.21×10^{-2}	-0.91×10^{-5}
		300	115.95	-0.87×10^{-1}	0.55×10^{-3}	0.19×10^{-5}
		400	103.59	-0.14	0.21×10^{-4}	0.39×10^{-6}
		500	89.35	-0.14	-0.94×10^{-4}	0.32×10^{-6}

These values allow the determination of martensite plate profile characteristics (width and height) for any intermediary number of air-training cycles, up to 500, for both elongated and compressed areas, while considering the effects of oil-cycling. In addition, the average values of width and height corresponding to central solid lines in Figs. 5 and 6 can be calculated.

The deviations of mean measured values of widths and heights, with reference to the width and height values, respectively, determined by the general variation tendencies of these surface profile characteristics were further calculated. Their evolution is illustrated in Fig.7.

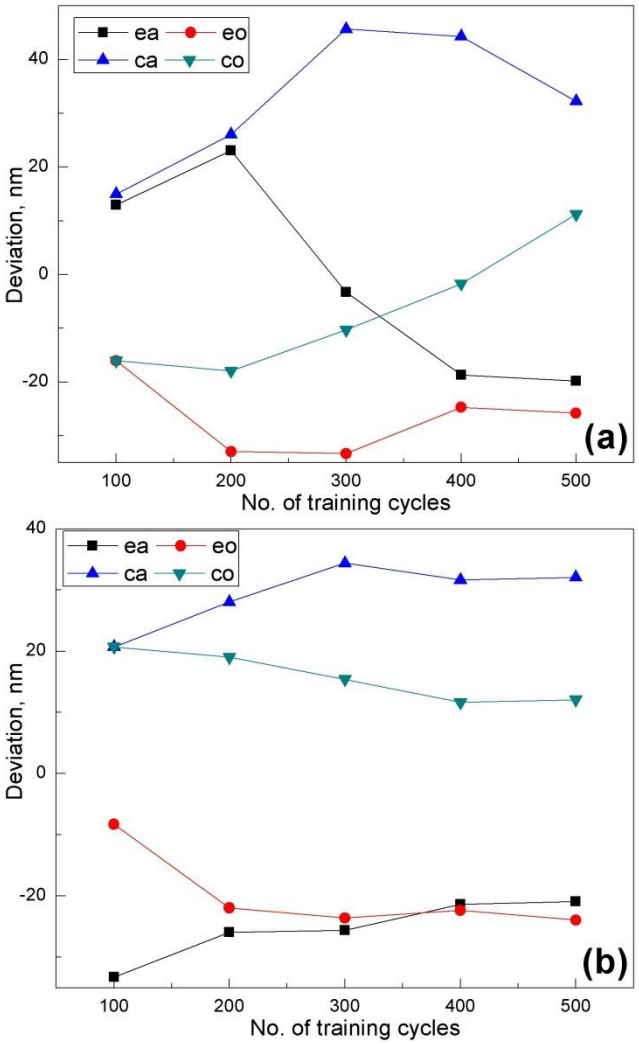

Fig. 7. Evolutions of the deviations of average measured values with reference to the values determined by the general variation tendency of martensite plates: (a) widths and (b) heights.

In Fig. 7 the values corresponding to elongated areas after air-training and oil-cycling are designated as *ea* and *eo*, respectively. For compressed areas the corresponding values were designated as *ca* and *co*.

By analysing Fig. 7, it is obvious that the values of martensite plate profiles measured on compressed areas, after oil-cycling, *co*, display the lowest deviations from general variation tendencies. These deviations are approx. ± 15 nm for martensite plate widths and 12-20 nm for heights. For the rest of loading modes and cycling environments the deviations were larger. However, they never exceed the range -32, … +45 nm.

4. Summary and conclusions

A comparative structural analysis, on the effects of the number of training cycles, loading mode and environment on the surface relief profile of martensite plates, was performed by means of AFM investigations, comprising the study of 2D and 3D representative profiles. The qualitative evaluation depicted that martensites plates were refined with increasing the number of training cycles and after oil-cycling, mostly as an effect of the occurrence of secondary martensite population of plates.

From the point of view of the numerical method, spline interpolation was preferred, taking into account (among other things) the qualitative aspects concerning the interpolation error. As it is well known, this error can be small even when using a spline of a lower degree. Spline interpolation enabled to develop two relationships for the general variation tendencies of martensite plate widths and heights, with increasing the number of training cycles up to 500.

Acknowledgements

This research work was supported by the project PN-II-ID-PCE-2012-4-0033, contract 13/ 2013.

References

[1] J. Cederstrom, V. Kolomytsev, A. Kozlov, P. Titov, G. Zatulskii, S. Kondratjuk, Materials Science and Engineering, A, 804, 273 (1999).
[2] J. Ilczuk, B. Kostrubiec, H. Morawiec, J. Rasek, Journal of Alloys and Compounds, **201**, 211 (1994).
[3] L. Sun, W.M. Huang, Z. Ding, Y. Zhao, C.C. Wang, H. Purnawali, C. Tang, Materials & Design, **33**, 577 (2012).
[4] H. Scherngell, A. C. Kneissl, Mater. Sci. Eng. A, **400**, 273 (1999).
[5] X.M. Zhang, M. Liu, J. Fernandez, Mater. Des., **21**, 557 (2000).
[6] R. Stalmans, J. Van Humbeeck, L. Delaey, Acta Metall. Mater., **40**, 2921 (1992)
[7] H.W. Kim, J. Mater. Process. Technol., **146**, 326 (2004).
[8] Y. Zhang, S. Jiang, L. Hu, Y. Liang, Materials Science and Engineering: A, **559**(1), 607 (2013).
[9] M. Eskil, N. Kayali, Materials Letters, 60 (5), 630 (2006).
[10] C.Y. Chung, C.W.H. Lam, S.S. Tan, Materials Letters, **33** (5–6), 291 (1998).
[11] A. Planes, F. J. Pérez-Reche, E. Vives, L. Mañosa, Scripta Materialia, **50** (2), 181 (2004).
[12] M. Ahlers, Prog. Mater. Sci., **30**, 135 (1986).
[13] F. Lanzini, R. Romero, G.H. Rubiolo, Calphad, 35(3), 396 (2011).
[14] O. Adiguzel, Journal of Materials Processing Technology, **185**(1–3), 120 (2007).
[15] L.G.Bujoreanu, Mat Sci Eng A, **395**, 481(2008).
[16] J. Perkins, K. Adachi, M.-H. Wu, T. Yamashita, Ultramicroscopy, **30**(1–2), 217 (1989).
[17] L.G.Bujoreanu, M.L.Craus, S.Stanciu, V.Dia, Mater Sci Tech Lond, **16**(June), 612 (2000).
[18] D.P. Dunne, G.W. Delamore, J.H. Zhu, Ecomaterials, 935, 1994..
[19] J. M. Guilemany, B. G. Mellor, J. Fernández, Materials Letters, **13**(2–3), 105 (1992).
[20] L.-G. Bujoreanu, S. Stanciu, A. Enache, C. Lohan, I. Rusu, J Optoelectron Adv M, **10**(3), 602 (2008).
[21] A. Amengual, V. Torra, Thermochimica Acta, **198**(2), 381 (1992).
[22] F. C. Bubani, M. Sade, F. Lovey, Materials Science and Engineering: A, **577**, 147 (2013).
[23] G. Vitel, A. L. Paraschiv, M. G. Suru, N. Cimpoesu, L.-G. Bujoreanu, Optoelectron Adv Mat, **5**(8), 858 (2011).
[24] G. Vitel, A. L. Paraschiv, M. G. Suru, N. Cimpoesu, L.-G. Bujoreanu, Optoelectron Adv Mat, **6**(1-2), 339 (2012).
[25] M. G. Suru, A. L. Paraschiv, B. Pricop, L. G. Bujoreanu, Optoelectron Adv Mat, **7**(1-2), 141 (2013).
[26] L. G. Bujoreanu, N. M. Lohan, B. Pricop, N. Cimpoeşu, J Mater Eng Perform, **20**(3), 468 (2011).
[27] G. Vitel, M. G. Suru, A. L. Paraschiv, N. M. Lohan, B. Pricop, M. Baciu, L. G. Bujoreanu, Mater Manuf Process, **28**(1), 79 (2013).
[28] M.-G. Suru, I. Dan, N. M. Lohan, A. L. Paraschiv, B. Pricop, I. P. Spiridon, C. Baciu, L.-G. Bujoreanu, Materialwiss Werkst, **45**(1), 44 (2014).
[29] C. Moroşanu, Bentham Science Publishers, 185, 2012.
[30] M.-G. Suru and L.-G. Bujoreanu, Materialwiss Werkst, **43**(11), 973 (2012).
[31] C. Moroşanu, ROMAI J., **8**(1), 73 (2012).
[32] C. Moroşanu, PanAmerican Math. J., **12**(2), 31 (2002).

*Corresponding author: lgbujor@yahoo.com